

Concentrating colloids with electric field gradients. I. Particle transport and growth mechanism of hard-sphere-like crystals in an electric bottle

Mirjam E. Leunissen,^{1,a),b)} Matthew T. Sullivan,^{2,3,c)} Paul M. Chaikin,^{2,3,a)} and Alfons van Blaaderen^{1,d)}

¹*Soft Condensed Matter, Debye Institute for Nanomaterials Science, Utrecht University, Princetonplein 5, 3584 CC Utrecht, The Netherlands*

²*Princeton Institute for the Science and Technology of Materials, Princeton University, Princeton, New Jersey 08534, USA*

³*Department of Physics, Princeton University, Princeton, New Jersey 08534, USA*

(Received 10 December 2007; accepted 21 March 2008; published online 22 April 2008)

This work concerns the use of electric field gradients to manipulate the local particle concentration in a hard-sphere-like suspension. Inside a specially designed “electric bottle,” we observed our colloids to collect in the regions of lowest field strength (“negative dielectrophoresis”). This allows for the use of larger field gradients and stronger dielectrophoretic forces than in the original electric bottle design, which was based on positive dielectrophoresis [M. T. Sullivan *et al.*, Phys. Rev. Lett. **96**, 015703 (2006)]. We used confocal scanning laser microscopy to quantitatively follow the time-dependent change in the particle density and the suspension structure. Within a few days, the dielectrophoretic compression was seen to initiate a heterogeneouslike growth of large single crystals, which took place far out-of-equilibrium. The crystals had a random hexagonal close-packed structure and displayed an intriguing growth mechanism, during which the entire crystal was continuously transported, while growing both on the “high-field” and the “low-field” sides, although at different rates. After switching off the electric field, the compressed crystals were found to relax to a lower packing fraction and melt, at a much slower rate than the crystal growth. Besides revealing the particular (far out-of-equilibrium) crystal growth mechanism in these electric bottles, our observations also shed light on the role of the different particle transport processes in the cell and some of the relevant tuning parameters. This is useful for different types of experiments, for instance, focusing more on melting, homogeneous crystallization, or the glass transition. © 2008 American Institute of Physics. [DOI: 10.1063/1.2909198]

I. INTRODUCTION

In almost all soft matter systems, such as foams, (bio)polymers, emulsions, and liquid crystals, the relative concentrations of the different constituting species are of great importance for the overall behavior. For colloidal suspensions of so-called hard spheres, which only have a repulsive excluded volume interaction, the particle concentration is the only parameter that controls the phase behavior.¹ Recently, Sullivan *et al.* demonstrated for such hard-sphere suspensions how dielectrophoretic forces can be employed to manipulate the local particle concentration inside a relatively small, sealed sample cell.^{2,3}

Dielectrophoresis (DEP) is the translational motion of particles induced by an inhomogeneous electric field.⁴ A particle with a dielectric constant (ϵ_p) different from the suspending medium (ϵ_m) acquires a dipole moment, which then is either attracted toward (for nonconductive media if $\epsilon_p > \epsilon_m$, “positive” DEP), or repelled from (for nonconductive

media if $\epsilon_p < \epsilon_m$, “negative” DEP) the areas with the strongest electric field. In the past decades, a large variety of dielectrophoretic techniques has been used for a diverse range of purposes. For example, many companies have adapted DEP for the treatment of industrial streams, removing particulate matter from liquids and gasses.⁴ On a laboratory scale, it is frequently used for particle separation and characterization, especially in biology (cells).⁵ More recently, DEP has also found application in the manipulation of single molecules⁶ and the directed assembly of micro- and nanoscale structures.⁷ Many more novel applications can be expected in the near future, given the fast developments in the field of microfluidics. Moreover, DEP could be a convenient way to manipulate nanocrystals with permanent dipoles⁸ or complex colloids that are only available in small quantities.⁹

As Sullivan *et al.* pointed out,³ most of the existing applications are aimed at dilute suspensions, in which individual particles or small collections of them are being moved around. In contrast, they showed that the combination of dielectrophoretic forces and confinement gives good control over the local particle concentration in more concentrated colloidal suspensions. In their method, a finite, sealed system (coined “electric bottle”) is allowed to come to equilibrium under the action of an electric field gradient. When full equi-

^{a)}Present address: Center for Soft Matter Research, New York University, 4 Washington Place, New York, NY 10003, USA.

^{b)}Electronic mail: m.e.leunissen@nyu.edu.

^{c)}Present address: Department of Engineering and Applied Sciences, Harvard University, Cambridge, MA 02138, USA.

^{d)}Electronic mail: a.vanblaaderen@uu.nl.

librium is reached, the osmotic pressure balances the electrostatic driving force,¹⁰ as will be described in Sec. I.

Here, we will explore the electric bottle concept further, using hard-sphere-like suspensions as the simplest model system. It consists of sterically stabilized polymethyl methacrylate (PMMA) particles ($\varepsilon_p \approx 2.6$) suspended in a near density- and index-matched, salt-saturated mixture of the organic solvents cyclohexyl bromide and *cis*-decalin ($\varepsilon_m \approx 6-7$). In our solvent mixture, the particles collect in the regions of lowest field strength (negative DEP), in contrast with the situation in Ref. 3, where the particles got trapped in the high-field area (positive DEP). We will present a new sample cell layout, especially meant for the present case of negative dielectric constant contrast, and discuss the merits and drawbacks of negative versus positive DEP.

While Sullivan *et al.* gave a convincing demonstration of the usefulness of electric bottles, important questions regarding the mechanism of the externally driven crystal nucleation and growth were left unanswered. This is because in Ref. 3, only the final, steady-state particle distributions were studied. Therefore, in this paper, we will also focus on the evolution of the particle distribution in time and study the crystal growth and melting mechanisms in these electric bottles. To this end, we keep track of the changes in the suspension, both qualitatively and quantitatively, by means of confocal scanning laser microscopy on fluorescently labeled particles. We will show that this provides valuable insight in the different particle transport mechanisms at work, as well as the important control parameters and sample cell design principles.

The paper is organized as follows. Section I gives an overview of the theoretical principles underlying the concept of the electric bottle and shows how the expected equilibrium particle density profiles can be found computationally. Section II gives the experimental details, followed by a discussion of the experimental results in Section III and conclusions.

II. THEORETICAL BACKGROUND

As mentioned in the Introduction, colloidal particles experience a dielectrophoretic force \mathbf{F}_{dep} , when they are subjected to an inhomogeneous electric field $\mathbf{E}(\mathbf{r})$,¹¹

$$\mathbf{F}_{\text{dep}} = -\frac{1}{2}v_p\varepsilon_{\text{eff}}\varepsilon_0 \nabla |\mathbf{E}|^2(\mathbf{r}), \quad (1)$$

where ε_0 is the permittivity of vacuum, v_p is the volume of the particle, and $\varepsilon_{\text{eff}} = 3\beta\varepsilon_m / (1 - \beta\varphi)^2$ is the effective dielectric constant of the particle in the suspension [see the derivation of Eq. (9) below], with φ as the particle volume fraction, $\beta(\omega) = \text{Re}\{[\varepsilon_p^*(\omega) - \varepsilon_m^*(\omega)] / [\varepsilon_p^*(\omega) + 2\varepsilon_m^*(\omega)]\}$ taken at the frequency ω of interest, and $\varepsilon_p^*(\omega) / \varepsilon_m^*(\omega)$ the complex permittivity of the particles and the suspending medium, respectively. It is important to note two things about the dielectrophoretic force. First, the dielectrophoretic force depends on the square of the electric field, which means that it is independent of the field direction. This relationship allows the use of (high frequency) ac fields. In our experiments, we used a sinusoidal field with a frequency of 1 MHz to prevent polarization of the double layer and unwanted electrohydro-

dynamic effects. Second, the force depends both on the magnitude of the electric field (through the induced dipole) and the gradient of \mathbf{E}^2 . Thus, for a large dielectrophoretic force, one should use not only a strong electric field but also a steep field gradient, which is obtainable through the electrode layout.

The field-induced dielectrophoretic motion leads to accumulation of the particles, either in the areas with the highest electric field strength ($\beta > 0$), or in the areas with the weakest electric field ($\beta < 0$). This raises the osmotic pressure Π in these parts of the sample cell. In a finite, sealed system (an electric bottle), the spatial particle distribution will eventually reach an equilibrium state, when the induced osmotic pressure gradient exactly counterbalances the electrostatic driving force. In equation form, this equilibrium condition reads

$$\nabla \Pi = \frac{\varphi}{v_p} \mathbf{F}_{\text{dep}}, \quad (2)$$

with \mathbf{F}_{dep} from Eq. (1). Here, we assume that the field varies smoothly on the scale of the typical interparticle distance, so that we can use a local density approximation.

If the electric field profile is known, the expected equilibrium particle distribution can be obtained from the above pressure balance or from equating the chemical potential μ throughout the system; here, we will use the latter approach. The predicted particle distribution can then be used to verify if equilibrium has been reached in the experimental system (see Sec. IV).

In the presence of an external potential, we can write the Helmholtz free energy as

$$F = F_0 + \Phi, \quad (3)$$

with F_0 as the internal free energy of the suspension in the absence of external fields and Φ as the free energy contribution due to the external potential. As Φ is extensive, we can also write $\Phi = -WV$, where W is the increase in electrostatic energy per unit volume V of the suspension due to the applied electric field $\mathbf{E}(\mathbf{r})$ [see also Eq. (6) below]. From the definition $\mu = (\partial F / \partial N)_{T,V}$ and the fact that the number of particles $N = \varphi V / v_p$, it follows that the total chemical potential is

$$\mu = \mu_0 - v_p \left(\frac{\partial W}{\partial \varphi} \right)_{T,V}. \quad (4)$$

Here, μ_0 is the internal chemical potential of the suspension and the second term is the change in chemical potential due to the external electric field.

Inside the electric bottle there is a free particle exchange, so that in the eventual equilibrium state, the total chemical potential will be the same everywhere, $\mu = \mu_0^0$. The constant μ_0^0 is not known *a priori*, but it follows from the requirement of conservation of the total particle number. Thus, starting with an initially homogeneous particle distribution, $\varphi_i(\mathbf{r}) = \varphi_0$, the final, field-induced density profile $\varphi_f(\mathbf{r})$ must satisfy the condition that

$$\int_{V_s} \varphi_f(\mathbf{r}) d\mathbf{r} = \varphi_0 V_s, \quad (5)$$

where V_s is the volume occupied by the suspension.

Because W reflects the total increase in electrostatic energy due to the applied electric field, it encompasses both the interaction of the individual particles with the external field and the induced dipole-dipole interactions between the particles. For aligned dipoles that are isotropically distributed, the dipole-dipole interaction averages to zero and only the macroscopic electrostatic energy is important. Thus, for small electric fields, the symmetry of the colloidal fluid between the electrodes remains unaffected and the system may be treated as an effective dielectric. Then, macroscopic electrodynamics gives

$$W = \frac{1}{2} [\varepsilon_s(\varphi) - \varepsilon_m] \varepsilon_0 \mathbf{E}^2, \quad (6)$$

where ε_s is the volume fraction dependent effective suspension dielectric constant. The advantage of this approach is that ε_s can, in principle, be experimentally measured. However, there also exist good theoretical approximations. Here, we will use the mean-field Maxwell–Garnett relation for an isotropic suspension with a small difference in dielectric constant between the particles and the suspending solvent ($|\beta\varphi| \ll 1$),¹²

$$\varepsilon_s = \varepsilon_m \frac{(1 + 2\beta\varphi)}{(1 - \beta\varphi)}. \quad (7)$$

This approximation takes into account that the local electric field that a particle experiences will be different from the externally applied field.

Using Eqs. (4), (6), and (7), together with the condition that the chemical potential has to be the same everywhere, we can now write the following equilibrium expression for the chemical potential:

$$\mu_0 = v_p \left(\frac{\partial W}{\partial \varphi} \right)_{T,V} + \mu_0^0 = \frac{1}{2} v_p \varepsilon_{\text{eff}}(\varphi) \varepsilon_0 \mathbf{E}^2(\mathbf{r}) + \mu_0^0, \quad (8)$$

with ε_{eff} as the effective, volume fraction dependent, particle dielectric constant:

$$\varepsilon_{\text{eff}} = 3 \frac{\beta \varepsilon_m}{(1 - \beta\varphi)^2}. \quad (9)$$

Note that this is the effective particle dielectric constant that appears in Eq. (1); it ensures that we can use Eq. (1) for the dielectrophoretic force as it accounts for all particle-particle interactions in our dense suspensions. Another, more well-known expression for the effective particle dielectric constant is the mean-field Clausius–Mossotti equation, $\varepsilon_{\text{eff}} = 3\beta\varepsilon_m$ (Ref. 13). However, this expression is only valid for low particle volume fractions and low field strengths.

Equation (8) can be numerically inverted to yield the particle-density distribution $\varphi_f(\mathbf{r})$ once $\varepsilon_s(\varphi)$, $\mathbf{E}(\mathbf{r})$ (determined by the experimental geometry and the local dielectric constant) and $\mu_0(\varphi)$ are known. The latter, the so-called “equation of state” of the colloidal system, can be obtained from different theoretical approximations, depending on the nature of the particle interactions. For hard spheres, with

only an excluded volume interaction, the theoretical equations of state for the liquid and crystalline phases are accurately known.¹⁴ We point out that the local coarse-grained dielectric constant will change when the local volume fraction of the particles changes because their dielectric constant is different from that of the suspending solvent. This spatial variation of the suspension dielectric constant affects the electric field profile. Therefore, the procedure described above should be iterated to find a self-consistent result for the $\mathbf{E}(\mathbf{r}) - \varphi(\mathbf{r})$ couple.

We employed the freely available Poisson SUPERFISH package¹⁵ to calculate the [two-dimensional (2D)] electric field profile in a representation of our experimental sample cell (which includes the glass walls, the electrodes, and the sample space with the volume fraction dependent suspension dielectric constant), using a successive over-relaxation method. From this solution, we extracted the electric field strength at all points inside the sample space and then calculated the local chemical potential of the particles, adding up the internal and external contributions. Finally, we computed the new particle distribution, which served as the input for the next iteration. The iterations were continued until the electric field and particle-density profiles were found to be stationary (typically taking about four iterations).

III. EXPERIMENTAL DETAILS

A. Sample cells

We used two different electric bottle designs: One with a “slit-like” and one with a “square” geometry. The slit cell consisted of two parallel-plate capacitors of approximately 2 mm wide, with a 2 mm wide electrode-free slit in between [Fig. 1(a)]. The electrode carrying slides were 1 glass cover slips ($22 \times 22 \text{ mm}^2$, 130–160 μm thick, $\varepsilon_g = 6.7$ at 1 MHz; Menzel) and the spacers, which also formed the side walls, were cut out of slides 0 (80–120 μm thick). The cell was constructed on top of a 1.0 mm thick microscopy slide, for extra support and easy mounting on the stage of the microscope. The entire assembly was secured with a UV-curing optical adhesive (Norland No. 71). After filling the cell with the colloidal suspension, it was sealed with a more viscous optical adhesive (Norland No. 68). The semitransparent indium tin oxide (ITO) electrodes were deposited in-house. Placing them on the outside of the sample cell not only facilitated wiring of the cell but also prevented unwanted electrohydrodynamic instabilities at the electrode edges due to electrode-suspension contact. For the electrical contacts on top of the ITO electrodes, we used silver paint (Jeol) and thin T2 thermocouple alloy wire (diameter of 50 μm , Goodfellow), which was then wrapped around standard electronic wire. The other sample cell design had a square electrode-free area of approximately $2 \times 2 \text{ mm}^2$. We constructed the cell in the same way as the slit cell, but now with spacers 00 (thickness of 55–80 μm). The semitransparent electrodes were fabricated by sputter deposition of 3 nm chromium, followed by 9 nm gold (Cressington, 208 h), while covering part of the glass slide with a square piece of Scotch tape.

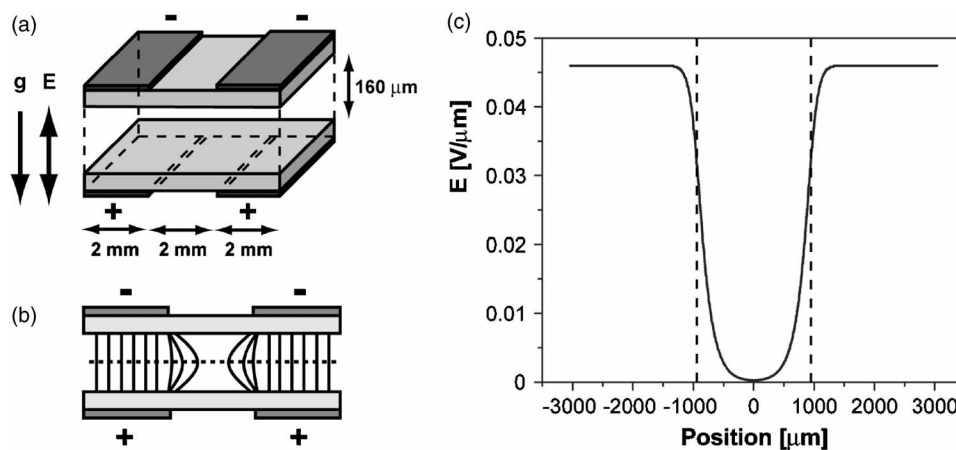


FIG. 1. (a) Schematic drawing of the electric bottle. The $\sim 150 \mu\text{m}$ thick glass slides (light gray) and the very thin electrodes (dark gray) are not drawn to scale. The respective directions of gravity and the (ac) electric field when the cell was mounted on the stage of the microscope are indicated with arrows. (b) Schematic side view of the cell, with an artistic impression of the contour lines of the electric field. The dotted line indicates the position, halfway the height of the sample space, for which the profile in panel (c) was drawn up. (c) Electric field profile calculated at an applied voltage $V_{\text{rms}} = 17.7 \text{ V}$. The dashed lines indicate the position of the slit edges (see text for all the relevant parameters).

B. Suspensions

We used nearly density and refractive-index matched suspensions of PMMA [1.19 g/ml , $\epsilon_p \approx 2.6$ at 1 MHz (Ref. 16)] particles, covalently labeled with the fluorescent dye rhodamine isothiocyanate and sterically stabilized with poly(12-hydroxystearic acid). We synthesized these particles by means of dispersion polymerization.¹⁷ The particles had a diameter of $2.20 \mu\text{m}$ and a size polydispersity of 3%, as determined from static light scattering measurements. The solvent mixture consisted of as received cyclohexyl bromide (CHB) (1.33 g/ml , Fluka) and *cis*-decalin (0.89 g/ml , Sigma-Aldrich). We saturated it with tetrabutylammonium bromide salt (Sigma-Aldrich) to screen the charges on the particles as much as possible, ensuring hard-sphere-like behavior.¹⁸ The PMMA particles were observed to selectively absorb a small fraction of the CHB from the mixture, which changed their effective density and dielectric constant (thereby changing their polarizability). Therefore, we let the suspensions equilibrate for several days before filling the sample cells. The slit cell was filled with an overall particle volume fraction $\varphi = 0.31$ in a mixture of CHB and 13.74 wt % decalin. The suspension in the square cell had the same particle volume fraction, but a 21.58 wt % decalin concentration. The dielectric constants of the particle-free solvent mixtures (ϵ_m) were 6.7 and 6.0, respectively, as determined through correlation with the measured refractive indices of several mixtures and the pure CHB and *cis*-decalin solvents.¹⁹

C. Data acquisition and analysis

We studied our samples using confocal scanning laser microscopy (Leica NT CSLM with numerical aperture (NA) of 1.3, $63\times$ and NA of 1.25, $40\times$ oil immersion objectives and 568 nm excitation) and a modified microscope stage (Rolyn, 750-MS) with low-speed closed-loop motorized actuators (Newport, 850G-LS) for accurate positioning. Sullivan *et al.* determined the local particle volume fraction by comparing 2D images with a sample of known volume

fraction.³ Although the use of 2D data would speed up the data acquisition, we chose to use three-dimensional (3D) data, consisting of a stack of xy slices. This provides for more flexibility in the choice of particles and is less sensitive to the particle interactions, the cell design (especially the light absorption by the electrodes) and the imaging conditions (for example, the laser power and magnification). We took data stacks between 30 and $50 \mu\text{m}$ above the bottom of the sample cell and extracted the 3D particle coordinates with an adapted version of the method of Crocker and Grier²⁰ as it was described by Royall *et al.*²¹ A single data stack consisted of $128 \times 128 \times 48$ pixels, which took around 20 s of scanning. The xy pixels were $220 \times 220 \text{ nm}^2$ in size, and the separation between the xy slices was 440 nm . We took these data stacks at regular distances across the entire width of the cell to obtain the complete volume fraction profile.

IV. RESULTS AND DISCUSSION

A. Dielectrophoretic force and dipole-dipole interactions

Figures 1(a) and 1(b) present a schematic drawing of our electric bottle with a slitlike geometry for negative DEP. The cell consists of two parallel-plate capacitors with an electrode-free slit in between and basically is an “inverted” version of the sample cell used in Ref. 3, viz., with respect to the electrode configuration. To determine the exact position of the slit edges in our sample cell, we used both bright field transmission and confocal microscopy. With the latter technique, we looked for the slight increase in fluorescence intensity of the suspension when one moves into the slit. In this way, the position of the slit edges was found to be $\pm 960 \mu\text{m}$, setting the center of the slit to 0. We estimated the height of the sample space enclosed by the cover slips to be $\sim 160 \mu\text{m}$.

Following the procedure described in Sec. II, we calculated the electric field profile for this cell geometry as it would be at the start of the experiment, i.e., the dielectric

constant of the sample space was taken to be that of a homogeneous, isotropic suspension (ϵ_s), with a particle volume fraction $\varphi=0.31$ (from particle tracking). Equation (7) then gives $\epsilon_s=5.2$, when $\epsilon_m=6.7$ and $\beta=-0.26$. Figure 1(c) shows the resulting electric field profile halfway the height of the sample space, at the experimentally applied root mean squared voltage $V_{\text{rms}}=17.7$ V (at $\omega \approx 1$ MHz). As expected, there is a steep electric field gradient at the slit edges, providing the dielectrophoretic driving force, and a negligible field strength in the center of the slit ($\ll 0.01$ V μm^{-1}). The field strength between the electrodes is approximately 0.045 V μm^{-1} .

As the dielectric constant of our PMMA particles is smaller than that of the suspending solvent mixture ($\beta < 0$), they are driven toward areas with the lowest field strength and are thus compressed inside the “field-free” slit. This is a major advantage of systems based on negative DEP, as compared to positive DEP systems, like the one presented by Sullivan *et al.*, where the particles collected in areas of highest field strength.³ With the current layout, the risk of induced dipole-dipole interactions influencing the structure of the compressed suspension is much smaller, which means that we can use larger field gradients and thus larger dielectrophoretic driving forces. For the situation in Fig. 1(c), we find from Eq. (1) that the particles experience a dielectrophoretic driving force of -1.7×10^{-16} N, when they are at the maximum field gradient ($\nabla E = -7.4 \times 10^7$ V m^{-2} ; $|E| \approx 0.023$ V μm^{-1}). Here, we approximated the effective particle dielectric constant with Eq. (9), giving $\epsilon_{\text{eff}} = -4.4$. The use of very large fields may still have a drawback though, as it could lead to extensive dipole-induced structuring of the suspension between the electrodes (into “strings” and crystalline phases, see Refs. 18 and 22), thus hampering compression by slowing down the particle motion. However, at the experimental field strengths used below, we did not observe the formation of any strings longer than about two to three particles between the electrodes. Finally, we point out that the collection of particles in the low-field areas of a negative DEP system has as another advantage that they are not obscured by the electrodes. This makes it easier to study the suspension with (confocal) microscopy and it offers, for instance, the possibility to manipulate individual particles with optical tweezers, without heating problems due to absorption of the laser light by the electrodes.¹⁹

B. Crystal growth

At the start of the compression experiment, the entire sample was a dense colloidal fluid, with an overall volume fraction of $\varphi=0.31$, as determined from particle tracking. In 12 days' time at $V_{\text{rms}}=17.7$ V, the entire field-free slit became crystalline, while the suspension between the electrodes remained a fluid. During this time, no crystallization or sedimentation was observed in a reference cell of similar geometry, but without an applied electric field. Thus, the observed fluid-crystal transition was entirely due to dielectrophoretic compression. The bright Bragg reflections in Fig. 2 reveal how the crystals nucleated at the two opposing slit edges and then continued to grow inward, until they met at

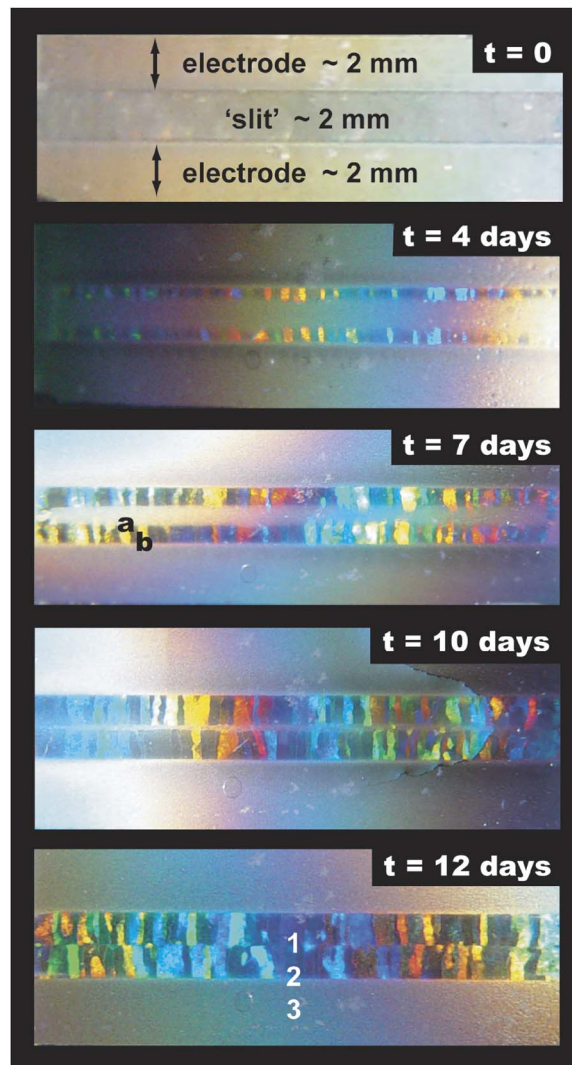


FIG. 2. (Color online) Bragg reflection images showing the crystallization induced by dielectrophoretic compression at $V_{\text{rms}}=17.7$ V [refer to Fig. 1(c) for the corresponding electric field strength at the different positions in the sample cell]. The bright reflections set the crystals apart from the more diffusively scattering colloidal fluid. The symbols in the images at $t=7$ and 12 days indicate the positions of the confocal images shown in Figs. 3 and 5. All photographs were taken in transmission using white-light illumination.

the center. During this growth process, the neighboring crystalline domains occasionally merged, but most of them remained distinguishable as separately reflecting entities. Figure 3 gives a qualitative impression of the induced particle-density profile after 12 days of compression.

Interestingly, while the crystalline bands steadily spread toward the center of the slit, the position of their outer edge remained nearly fixed (with “inner” edge of the crystalline band, we refer to the side that faces the slit center, the “outer” edge faces the electrodes). At first consideration, this behavior seems remarkable because the particles that are transported towards the slit by dielectrophoresis arrive at this side. The evolution of the local particle volume fraction (obtained from particle tracking) at different places in the sample cell provides more detail on this intriguing process (Fig. 4). These data were collected in another compression run with the same sample, after it had fully relaxed back to

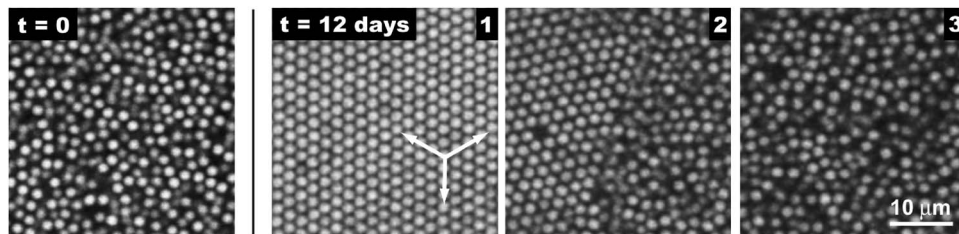


FIG. 3. Confocal microscopy images before ($t=0$) and after 12 days of compression at $V_{\text{rms}}=17.7$ V. The numbers correspond to different positions along the particle-density profile, as indicated in Fig. 2 ($t=12$ days). The arrows indicate the three equivalent close-packed directions of the hexagonal lattice.

the fluid state. We again started at $V_{\text{rms}}=17.7$ V, but raised the voltage to 26.5 and 35.4 V at later times [denoted as (1) and (2) in Fig. 4]. Within hours after turning on the electric field ($V_{\text{rms}}=17.7$ V), the particle volume fraction just outside the slit was reduced considerably, as these nearby particles were quickly driven into the slit. This was accompanied by a rapid increase in the particle density just inside the slit. This also turned out to be the place where the first crystals nucleated, after about 50 h. These crystals had a packing density of $\varphi_{\text{crys}}=0.44$, which we assume was (close to) the bulk crystallization volume fraction of this nearly hard-sphere suspension [a truly hard-sphere system is crystalline for $\varphi \geq 0.545$, for $\varphi \leq 0.494$ it forms an isotropic fluid, and in between the two phases coexist; (see Refs. 1 and 23)].

The particle concentration at the center of the slit increased much more slowly (curve I in Fig. 4). After 95 h, the crystals at the edges spanned the entire sample height already, while the central area was still a fluid, with nearly the same volume fraction as at the start of the experiment (note that in this run the starting volume fraction was $\varphi=0.39$, due to a slight sedimentation). Only after some 200 h, and raising the voltage to $V_{\text{rms}}=26.5$ V, the center did reach the bulk crystallization volume fraction of $\varphi \approx 0.44$. Eventually, however, when the entire slit had turned into a somewhat compressed crystal, it had a single volume fraction ($\varphi \approx 0.53$) throughout, as one would expect. At this time, the volume fraction of the colloidal fluid just outside the slit had dropped all the way to $\varphi=0.19$.

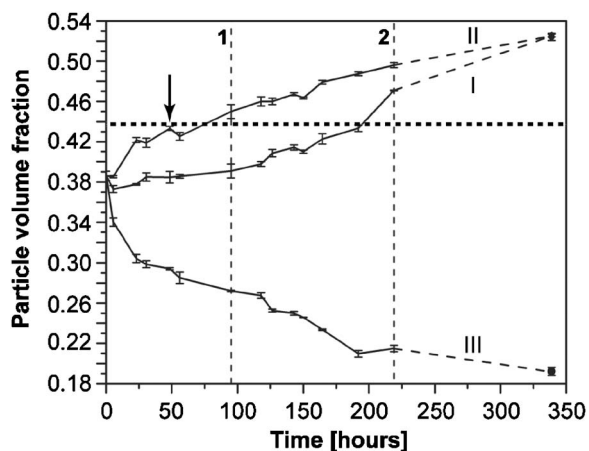


FIG. 4. The change in the particle volume fraction during dielectrophoretic compression at three different positions in the sample cell. Curve I was the center of the slit (position 0), curve II was just inside the slit ($750 \mu\text{m}$), and curve III was just outside the slit ($1250 \mu\text{m}$). The lines connecting the data points are meant as a guide to the eye. The vertical dashed lines indicate the course of the experiment, after turning on $V_{\text{rms}}=17.7$ V at $t=0$. (1) Field raised to $V_{\text{rms}}=26.5$ V; (2) field increased further to $V_{\text{rms}}=35.4$ V. The volume fraction of the first crystals (at the arrow) is also indicated (horizontal dotted line). All error bars are based on three repeat measurements.

Let us now consider the particle transport mechanisms that play a role in our electric bottle. First of all, particles near the edge of the electrodes are transported relatively quickly into the slit by the dielectrophoretic force that results from the local electric field gradient. We can get a feeling for this time scale by calculating the dielectrophoretic drift velocity of a single particle when it experiences the largest field gradient (for $V_{\text{rms}}=17.7$ V): $v_{\text{dep}}=F_{\text{dep}}/6\pi\eta a=3.6 \times 10^{-9} \text{ m s}^{-1}$, with a as the particle radius and η as the viscosity of the suspending solvent ($\sim 2.2 \times 10^{-3} \text{ Pa s}$). A single particle would thus take about 40 h to travel from the outermost point of the field gradient into the slit, a distance of $\sim 500 \mu\text{m}$. Of course, this is an approximation because in our dense suspensions the dielectrophoretic transport will be a collective process. Inside the slit, the electric field strength quickly drops to almost zero. At this point the distance to the center of the slit still is $\sim 600 \mu\text{m}$, which needs to be covered by collective diffusion without dielectrophoretic driving force (but driven by concentration differences). A full calculation of the time-dependent particle fluxes is beyond this paper because the occurrence of crystallization and pluglike motion of the entire crystal (see below) complicate matters. However, from the experimental observations, it is clear that the spreading of the particles over the field-free region occurs on a time scale of days to weeks, rather than hours to days, leading to the observed accumulation of particles at the slit edges. Eventually, when the system has reached full equilibrium, the particle distribution inside the field-free slit will be homogeneous (see below) and the dielectrophoretic influx of particles will be exactly balanced by the outflux that is caused by the osmotic pressure gradient. In our case, most of the compression took place far out-of-equilibrium because we instantaneously turned on a large field gradient. In order to reach the same final situation through states that are much closer to equilibrium, one should increase the field much more slowly. This will then allow enough time for the particle distribution to relax inside the field-free region, thus preventing inhomogeneities in the slit. Obviously, this would change the crystallization process.

One question that is still unanswered is how the outer edge of the crystalline band can stay at nearly the same position, despite the rapid addition of particles to that side. Figure 5 provides the answer to this, showing an experiment in which we studied the growth and the motion of the crystal as a whole. First, we bleached a rectangle in the colloidal crystal by scanning for several minutes at high laser power. This rectangle then served as a “landmark,” so that we could follow the growth and motion of the crystal over a prolonged time. In this way, the entire crystal was seen to move into the slit at an average speed of $\sim 0.5 \mu\text{m/h}$ ($V_{\text{rms}}=17.7$ V), while

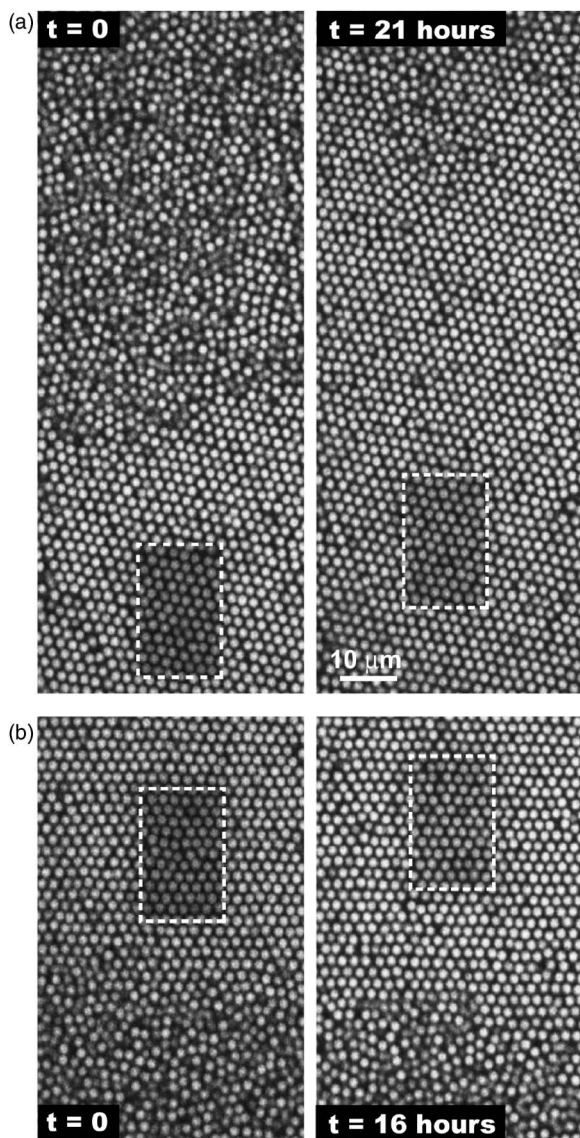


FIG. 5. Confocal microscopy images showing the simultaneous growth and motion of the crystalline bands (at $V_{\text{rms}}=17.7$ V). (a) Inner edge (slit center at the top side), and (b) outer edge (electrodes at the bottom side), as was indicated in Fig. 2 ($t=7$ days). The dashed lines highlight the circumference of a bleached patch, which served as a landmark.

it grew both at its inner and outer edge. More precisely, a rectangle near the outer edge [Fig. 5(b)] was displaced over $7 \mu\text{m}$ in 16 h, and at the same time, the crystal grew by $7 \mu\text{m}$ (two to three rows of particles) on this side. Repeating the experiment near the inner edge [Fig. 5(a)], resulted in a comparable displacement of $14 \mu\text{m}$ in 21 h. However, in the meantime, the crystal grew by no less than $62 \mu\text{m}$ on this side. We did not observe any shear in the particle planes (which would distort the rectangle) and hypothesize that the entire crystal moved as a solid “plug,” starting close to the walls.

To summarize our observations, the particles that were transported toward the slit by dielectrophoresis accumulated at the slit edges due to slow subsequent spreading. When the crystallization volume fraction was reached, the first crystallites appeared, which likely nucleated under influence of the wall. After this, no more nucleation took place and newly

arriving particles were instead added to the outer edge of the existing crystalline band. At the same time, however, the entire crystal was transported as a solid plug toward the center of the slit, on its way incorporating the particles in the central area, which added on to the inner edge.

C. Crystal characteristics

We now take a closer look at the crystals that grew in 12 days’ time at constant $V_{\text{rms}}=17.7$ V, and which were shown in Figs. 2 and 3 already. From the Bragg reflection images, it is immediately clear that the final crystalline domains were large and regular in shape. From confocal microscopy, we find a typical domain length of about $1150 \mu\text{m}$ and widths in the range of $250\text{--}900 \mu\text{m}$. Crystallites with a single orientation basically extended all the way from the slit edge to the center. Here, they met, but they did not reorient to fuse into a single crystal with the crystallites that grew from the other side. All crystallites consisted of a stacking of close-packed hexagonal layers, whose symmetry was perfect within the error of the confocal measurement, despite the anisotropic compression [for particles with a longer-ranged repulsion we do observe distortions under strong compression, (see Ref. 24)]. The fact that the close-packed (111) planes were oriented perpendicular to gravity and parallel to the bounding cover slips indicates that these structures are the result of heterogeneous(-like) crystal growth. It is now well established that hard-sphere crystals wet flat surfaces,²⁵ but nevertheless this growth mode has hardly been reported on in experimental hard-sphere-like systems. Likely, this is due to the fact that such crystals are usually easily disrupted by gravitational effects, as well as a lack of sufficiently fine control over the volume fraction, unlike the present electric bottle approach.

The stacking sequence of hexagonal layers can be denoted with the letters *A*, *B*, and *C*, indicating the three different possible, laterally shifted positions which the particles in every next layer can assume. To characterize a stack of multiple layers, it is common use to define an “overall stacking parameter” α in the following way:

$$\alpha = 1 - \frac{N_k}{N_l - 2}, \quad (10)$$

where N_l is the total number of layers and N_k is the number of “kinks.” Namely, if one looks at a cut through the stack of layers, an *ABC* sequence shows up as a continuous line, whereas an *ABA* sequence looks like a kink. The stacking parameter α is 1 for a perfect, continuous *ABC* or face-centered-cubic (fcc) stacking, 0 for a perfect *ABA* or hexagonal close-packed (hcp) stacking, and assumes intermediate values for more random sequences [“rhcp” random hexagonal close packed].^{26,27}

We analyzed 20 stacks of around 25 layers thick and found that $\alpha=0.61$ on average. We did not observe any values smaller than 0.50, nor ones larger than 0.75. Both the fcc and hcp sequences were mainly made up of short stacks of only three or four layers, although occasionally a thicker stack was observed (but never more than 15 layers). This occurred more often for the fcc than for the hcp sequence.

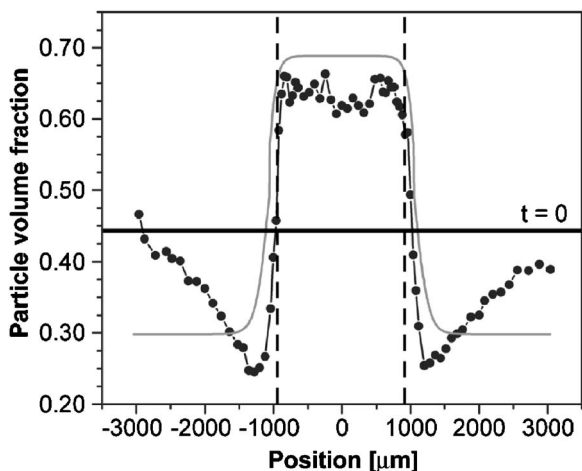


FIG. 6. Comparison of the experimental and calculated particle-density profiles after 12 days of compression at $V_{\text{rms}}=17.7$ V. Black dots: Experimental volume fractions mapped onto a hard-sphere suspension (see text); gray line: Calculated density profile for hard spheres. The scaled initial volume fraction is indicated with a solid black line ($t=0$) and the position of the slit edges with vertical dashed lines. The experimental data were obtained from particle tracking; the estimated error is $\sim 1\%$.

From this, it seems that if there was any preference for fcc stacking at all, that it then was a subtle effect only. Such a preference could be induced by the slight shear that the crystal experienced when it moved into the slit,²⁸ but it could also be a kinetic effect.²⁷ The observation of a rhcp structure agrees with the findings of other hard-sphere-like experiments, however.^{26,27}

What is also interesting is the distribution of angles between the slit edge and the close-packed directions of the hexagonal lattice. The latter are the directions in the (111) plane along which the particles (nearly) touch each other. These directions can be easily recognized in our confocal microscopy images (see Fig. 3). The maximum possible angle with respect to the slit edge is 30° because there are three equivalent directions with a 60° difference. Experimentally, there was a spread in angles, up to 25° , but there was a pronounced preference for small angles of $0\text{--}5^\circ$ (almost 60% of the data). The fact that the close-packed particle rows ran nearly parallel to the slit edge might be due to shear alignment of the crystals during the early nucleation and growth stages.²⁹

D. Rate of compression and equilibration

Figure 6 shows the particle-density profile across the sample cell after 12 days of compression at $V_{\text{rms}}=17.7$ V [at this time, the field-free slit had become fully crystalline (see Fig. 2)]. With a crystallization volume fraction of $\varphi \approx 0.39$ (the starting volume fraction was $\varphi=0.31$), our suspension was not completely hard-sphere-like, but did not have long-ranged repulsive particle interactions either. Therefore, we invoke an “effective hard-sphere diameter” σ_{eff} , and map the experimental volume fractions onto a hard-sphere suspension, which is characterized by a fluid-crystal coexistence at $\varphi=0.494\text{--}0.545$.^{1,23} Taking the new, scaled starting volume fraction $\varphi=0.44$ and the cell geometry presented above, we calculated the expected particle-density profile at dielectro-

phoretic equilibrium (i.e., constant chemical potential throughout the entire sample cell). We did this, following the procedure described in Sec. II, and using the hard-sphere equation of state.³⁰ We obtained the latter by integrating the Carnahan–Starling expression for the compressibility of the liquid, and the Hall expression for the crystalline state.¹⁴ The resulting hard-sphere density profile is shown as the gray line in Fig. 6.

When we compare the scaled experimental and the calculated density profiles, we see that the plateau value of the particle density inside the slit is quite comparable, as well as the steepness of the density gradient near the slit edges. This indicates that our particles indeed effectively behaved as hard spheres with a somewhat larger diameter, $\sigma_{\text{eff}}=2.47$ μm (versus 2.20 μm as determined by static light scattering). However, outside the slit, the theoretical profile is seen to quickly level off at $\varphi \approx 0.30$, whereas the experimental volume fraction first drops to $\varphi \approx 0.25$ and then increases again, going toward the side walls (± 960 μm). Likely, this is a consequence of the cell design: At the glass side walls there is another (weaker) field gradient, which “traps” some of the particles (we did not include this additional field gradient in our calculations). The positive DEP cell of Ref. 3 did not exhibit such behavior because the electrode pair was centered in the sample space, so that the electric field strength fell off well before the side walls. A general problem with parallel plate, capacitor-type cells like the ones used here and in Ref. 3, is the relatively short range of the field gradient. Here, the electric field gradient at the slit edges covered no more than 25% of the area between the electrodes [Fig. 1(c)]. Even though we could now use larger field gradients than in the positive DEP case, this design results in long equilibration times and relatively slow compression. This is because particles still need to travel large distances by diffusion without dielectrophoretic driving force.

Obviously, one can think of different ways to enhance the suspension compression in the capacitor-like negative DEP cells. One approach that we tested is the use of an electric bottle with a square electrode-free area (of approximately 2×2 mm^2). The rationale behind this design is that particles will be transported into the electrode-free area from four sides, instead of just two for the “slit” cell. We again applied a voltage of $V_{\text{rms}}=17.7$ V. However, in this case, the cell thickness was ~ 72 μm and is, therefore, much thinner than the previous design. Consequently, the dielectrophoretic force experienced by the particles in the “square cell” is estimated to be about five times larger (here, $\beta=-0.234$).

Within 1 day after energizing the cell, the first Bragg reflections of crystals became visible, just inside the edge of the field-free square, at $\varphi=0.44$. These were accompanied by a clearly lower particle concentration in a narrow band just outside the square, while the volume fraction of the fluid at the center was $\varphi=0.35$, still close to the starting value $\varphi=0.33$. All of this looked similar to the early stages of compression in the slit geometry. Again, the crystalline bands grew toward the center until the entire field-free area had become crystalline (Fig. 7), in a total time of 4 days. This is about three times faster than in our earlier experiment with

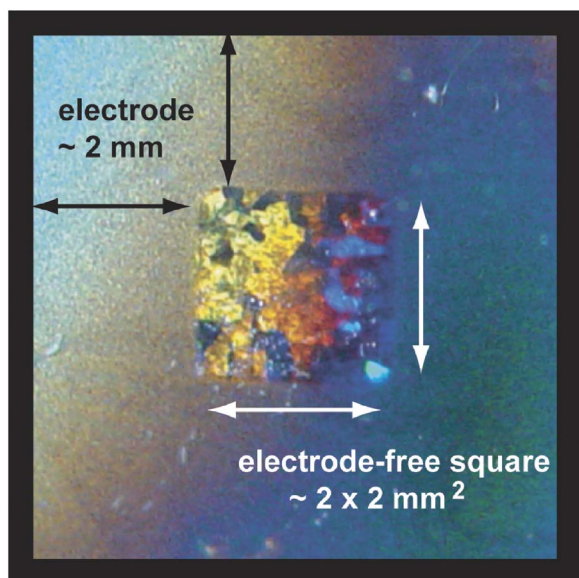


FIG. 7. (Color online) Bragg reflection image showing the crystal that was formed by 4 days of compression at $V_{\text{rms}}=17.7$ V in an electric bottle with a square geometry of the electrode-free area.

the slit cell (Fig. 2), but still slower than the expected total time of ~ 2.5 days that follows from the difference in dielectrophoretic force for the two cells. Note that for the latter estimate we did not even take into account the difference in geometry, which is expected to speed up the compression in the square cell even more (see above). One unknown, though, is the friction coefficient of the crystalline bands as they are pushed forward, which may depend on the geometry of the cell. Nevertheless, it is clear that in both geometries the rate of compression is severely limited by the short range of the field gradient at the electrode edges.

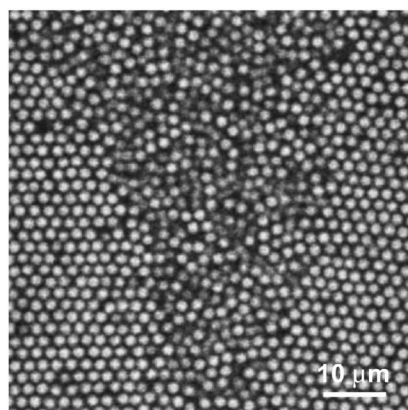
There was also a clear qualitative difference with the slit geometry in that the crystallites were more irregularly shaped in the square cell, with their dimensions ranging widely from ~ 125 to ~ 1360 μm . The less well-defined shape may be a result of the simultaneous compression and motion in mutually perpendicular directions but could also be caused by different nucleation conditions or by sedimentation. Unfortunately, the suspension was not as well density matched as the one in the slit cell, giving rise to small crystallites in a field-free reference sample. Although these crys-

tallites were much smaller than those in the electric bottle, they were also irregularly shaped. To prevent sedimentation in the electric bottle, as much as possible, we frequently turned it over during the compression (once every hour during the day). A possible influence cannot be entirely excluded, however.

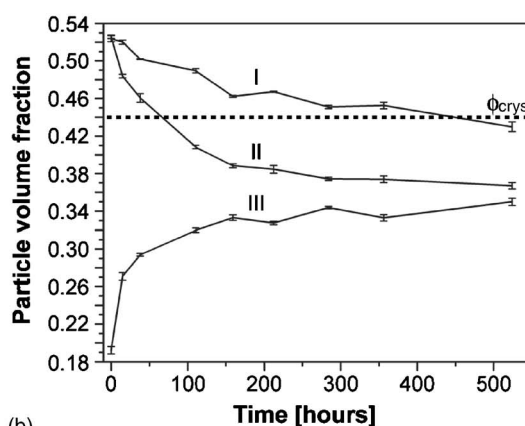
E. Melting

Because the heat of melting is negligibly small in colloidal systems, this process cannot be tuned with temperature in the same way as is possible for molecular systems. Only recently did Alsayed *et al.* succeed in studying the melting process in detail, by using strongly thermoresponsive microgel particles.³¹ In our electric bottle, it is rather easy to induce melting in a controlled way by adjusting the electric field gradient. We switched the electric field off instantaneously, causing the melting process to be far out-of-equilibrium. Nevertheless, the large crystal in the slit cell took weeks to months before it transformed back to the original colloidal fluid phase. Initially, the crystal started to melt at its outer edges and the melting process then slowly proceeded inward. During this process, the fluid-crystal interface became less well defined as compared to the dielectrophoretically driven crystal growth because the region of fluid-crystal coexistence broadened. The effects of the crystal slowly melting at its outer edges were especially apparent, where two differently oriented crystallites met, as the confocal micrograph in Fig. 8(a) shows. Apparently, the less ordered grain boundaries melted first, while the bulk of the crystallites remained well ordered for longer times. All of this is in accordance with the observations of Alsayed *et al.*, who saw that melting started at grain boundaries and dislocations in the bulk crystal when they drove an initially close-packed crystal of micro-gel particles toward the melting point.³¹ It is interesting to note that the boundary at the center of the slit, which was the last to crystallize in Fig. 2, eventually also opened up again. This again shows that the crystallites that grew from opposite sides of the slit did not fully merge in the final crystal.

We obtained more information on the melting process from another “growth and melt run,” the growth data of which were displayed in Fig. 4 already. We found that the melting of the crystal started off rapidly, at ~ 8.4 $\mu\text{m}/\text{h}$, but



(a)



(b)

FIG. 8. (a) Confocal micrograph of one of the outer edges of the melting crystal after 26 days at zero field. The slit edge ran parallel to the top side of the image. (b) The change in the particle volume fraction at three different positions in the sample cell after switching off the electric field ($V_{\text{rms}}=0$). Curve I is the center of the slit (position 0), Curve II is just inside the slit (750 μm), and Curve III is just outside the slit (1250 μm). The lines connecting the data points are a guide to the eye. The original volume fraction of the first crystals is also indicated. All error bars are based on three repeat measurements.

after approximately 40 h, it slowed down and then continued at a nearly constant rate of $\sim 1 \mu\text{m/h}$. Note that the latter is much slower than the observed growth rate under dielectrophoretic compression ($\sim 3.2 \mu\text{m/h}$ at 17.7 V and $\sim 8.3 \mu\text{m/h}$ at 26.5 V), because the osmotic pressure gradient only relaxes by expansion of the crystal lattice and collective diffusion without an additional external driving force. The relatively fast melting in the first 40 h is understandable when we take a look at the change in the local volume fraction just inside and just outside the slit, respectively at 750 and 1250 μm from the slit center [Fig. 8(b)]. In this figure, the local particle density minimum just outside the slit is seen to fill up quickly. At the same time, the volume fraction just inside the slit drops considerably, as these are the particles that go to the minimum. This relatively fast particle redistribution process slows down when the volume fractions on the in- and outside approach each other, thus slowing down the melting of the crystal. One can also see that it took the compressed crystal in the center of the slit about 480 h (20 days) to relax to the volume fraction at which originally the first crystals appeared ($\varphi=0.44$) and at which the crystal is in thermodynamic coexistence with the fluid phase. After this point, the volume fraction remained almost constant during the further shrinkage of the crystal, until it had entirely melted (not shown).

V. CONCLUSIONS

The recent work of Sullivan *et al.*^{2,3} gave a convincing demonstration of the usefulness of electric bottles, which confine colloidal particles by electric field gradients. It is a simple technique which provides much better (on/off) control over the particle concentration than, for instance, gravity and temperature gradients, and which is applicable to many different soft matter systems. Here, we have presented a cell design tailored for suspensions with a negative dielectric constant contrast. This has as a big advantage that particles collect in the electrode- and field-free area, facilitating their observation and enabling the use of larger dielectrophoretic driving forces. The design could still be further improved, however, by creating a broader electric field gradient. This could for instance be achieved with a wedge geometry of the electrodes³² or by constructing an array of cascaded electrodes.

Our study of the time-dependent changes in the suspension density and its structure has revealed an intriguing, far out-of-equilibrium, heterogeneous-like crystal growth mechanism, during which the entire crystal is continuously pushed inward while it grows. It also provides more insight in the dynamics and time scales of the particle transport processes, thus revealing that this growth mode was entered when the collective diffusion driven by gradients in the particle concentration could not keep up with the dielectrophoretic influx. This knowledge will help one to optimize the compression process, so as to achieve better quality crystals or an entirely different suspension behavior, such as homogeneous crystal nucleation or glass formation. Such fine tuning can, for example, be done by changing the applied electric field, the sample cell design, the particle size, or the dielectric

constants of the different constituents. However, even without minute fine tuning, dielectrophoresis has already proven to be a good technique to grow large, high-quality colloidal crystals at a well-controlled rate. It is also a promising method to obtain large crystals with a predefined orientation, using only a small templated area in the region where the crystals nucleate.³³ This could be interesting for applications, such as (electro-) optical devices. Finally, our preliminary results show that electric bottles could facilitate the study of melting, a process that until now has hardly been explored for colloidal systems.

ACKNOWLEDGMENTS

We thank A. D. Hollingsworth and W. B. Russel for facilitating the stay of M.E.L. at the Princeton Institute for the Science and Technology of Materials during the start-up of this research and H. D. Goldbach (Utrecht University) for the ITO deposition. This work was supported by the Stichting voor Fundamenteel Onderzoek der Materie, the Nederlandse Organisatie voor Wetenschappelijk Onderzoek and the National Aeronautics and Space Administration.

- ¹P. N. Pusey and W. van Meegen, *Nature (London)* **320**, 340 (1986).
- ²M. T. Sullivan, K. Zhao, C. Harrison, R. H. Austin, M. Megens, A. D. Hollingsworth, W. B. Russel, Z. D. Cheng, T. Mason, and P. M. Chaikin, *J. Phys.: Condens. Matter* **15**, S11 (2003).
- ³M. T. Sullivan, K. Zhao, A. D. Hollingsworth, R. H. Austin, W. B. Russel, and P. M. Chaikin, *Phys. Rev. Lett.* **96**, 015703 (2006).
- ⁴H. A. Pohl, *Dielectrophoresis: The Behavior of Neutral Matter in Non-Uniform Electric Fields* (Cambridge University Press, Cambridge, 1978).
- ⁵P. R. C. Gascoyne and J. Vykoukal, *Electrophoresis* **23**, 1973 (2002); R. Pethig, Y. Huang, X.-B. Wang, and J. P. H. Burt, *J. Phys. D* **24**, 881 (1992); H. Zhou, L. R. White, and R. D. Tilton, *J. Colloid Interface Sci.* **285**, 179 (2005); D. Holmes, H. Morgan, and N. G. Green, *Biosens. Bioelectron.* **21**, 1621 (2006).
- ⁶R. Hölzel, N. Calander, Z. Chiragwandi, M. Willander, and F. F. Bier, *Phys. Rev. Lett.* **95**, 128102 (2005).
- ⁷A. Docoslis and P. Alexandridis, *Electrophoresis* **23**, 2174 (2002); L. Zheng, S. Li, J. P. Brody, and P. J. Burke, *Langmuir* **20**, 8612 (2004); Y. Liu, J.-H. Chung, W. K. Liu, and R. S. Ruoff, *J. Phys. Chem. B* **110**, 14098 (2006).
- ⁸M. Shim and P. Guyot-Sionnest, *J. Chem. Phys.* **111**, 6955 (1999); S. Lin, M. Li, E. Dujardin, C. Girard, and S. Mann, *Adv. Mater. (Weinheim, Ger.)* **17**, 2553 (2005).
- ⁹V. N. Manoharan, M. T. Elsesser, and D. J. Pine, *Science* **301**, 483 (2003); P. M. Johnson, C. M. van Kats, and A. van Blaaderen, *Langmuir* **21**, 11510 (2005).
- ¹⁰B. Khusid and A. Acrivos, *Phys. Rev. E* **54**, 5428 (1996).
- ¹¹The theoretical background of the concept of dielectrophoretic equilibrium, as presented here, follows in broad lines the earlier treatments given by Pohl (Ref. 4), Khusid and Acrivos (Ref. 10), and Sullivan *et al.* (Ref. 3).
- ¹²S. S. Dukhin and V. N. Shilov, *Dielectric Phenomena and the Double Layer in Disperse Systems and Polyelectrolytes* (Wiley, New York, 1974).
- ¹³C. J. F. Böttcher, *Theory of Electric Polarization* (Elsevier, New York, 1952).
- ¹⁴N. F. Carnahan and K. E. Starling, *J. Chem. Phys.* **51**, 635 (1969); K. R. Hall, *ibid.* **57**, 2252 (1972).
- ¹⁵Los Alamos National Laboratory (http://laacg1.lanl.gov/laacg/services/download_sf.phtml).
- ¹⁶G. P. Mikhailov and T. I. Borisova, *Polym. Sci. U.S.S.R.* **2**, 387 (1961).
- ¹⁷G. Bosma, C. Pathmanoharan, E. H. A. de Hoog, W. K. Kegel, A. van Blaaderen, and H. N. W. Lekkerkerker, *J. Colloid Interface Sci.* **245**, 292 (2002).
- ¹⁸A. Yethiraj and A. van Blaaderen, *Nature (London)* **421**, 513 (2003).
- ¹⁹M. E. Leunissen, Ph.D. thesis, Utrecht University, 2007 (Available at <http://www.colloid.nl>).
- ²⁰J. C. Crocker and D. Grier, *J. Colloid Interface Sci.* **179**, 298 (1996).

- ²¹C. P. Royall, M. E. Leunissen, and A. van Blaaderen, *J. Phys.: Condens. Matter* **15**, S3581 (2003).
- ²²A.-P. Hynninen and M. Dijkstra, *Phys. Rev. Lett.* **94**, 138303 (2005).
- ²³W. W. Wood and J. D. Jacobson, *J. Chem. Phys.* **27**, 1207 (1957); B. J. Alder and T. E. Wainwright, *ibid.* **27**, 1208 (1957).
- ²⁴M. E. Leunissen and A. van Blaaderen, *J. Chem. Phys.* **128**, 164509 (2008).
- ²⁵M. Dijkstra, *Phys. Rev. Lett.* **93**, 108303 (2004).
- ²⁶P. N. Pusey, W. van Megen, P. Bartlett, B. J. Ackerson, J. G. Rarity, and S. M. Underwood, *Phys. Rev. Lett.* **63**, 2753 (1989); N. A. M. Verhaegh, J. S. van Duijneveldt, A. van Blaaderen, and H. N. W. Lekkerkerker, *J. Chem. Phys.* **102**, 1416 (1995); M. D. Haw, W. C. K. Poon, and P. N. Pusey, *Phys. Rev. E* **57**, 6859 (1998).
- ²⁷J. P. Hoogenboom, D. Derks, P. Vergeer, and A. van Blaaderen, *J. Chem. Phys.* **117**, 11320 (2002).
- ²⁸B. J. Ackerson and P. N. Pusey, *Phys. Rev. Lett.* **61**, 1033 (1988).
- ²⁹D. Derks, H. Wisman, A. van Blaaderen, and A. Imhof, *J. Phys.: Condens. Matter* **16**, S3917 (2004); D. Derks, Ph.D. thesis, Utrecht University, 2006 (available at <http://www.colloid.nl>).
- ³⁰Modeling the suspension as a system of scaled hard spheres may affect the computational results to a certain extent. Namely, the particle distribution depends on the volume of a particle v_p , the effective suspension dielectric constant $\epsilon_s(\varphi)$, and the electric field profile $E(r)$, all of which will change if one scales the experimental particle diameter. Nevertheless, the overall deviation from the “nonscaled” case is expected to be small because the changes partially cancel and the effective diameter is only $\sim 10\%$ larger than the real diameter here.
- ³¹A. M. Alsayed, M. F. Islam, J. F. Zhang, P. J. Collings, and A. G. Yodh, *Science* **309**, 1207 (2005).
- ³²K. Zhao, Ph.D. thesis, Princeton University, 2007.
- ³³A. van Blaaderen, R. Ruel, and P. Wiltzius, *Nature (London)* **385**, 321 (1997).